

Molecular modeling and 3D-QSAR studies of indolomorphinan derivatives as kappa opioid antagonists

Wei Li,^a Yun Tang,^{a,b,*} You-Li Zheng^a and Zhui-Bai Qiu^{a,*}

^aDepartment of Medicinal Chemistry, School of Pharmacy, Fudan University, 138 Yixueyuan Road, Shanghai 200032, China

^bSchool of Pharmacy, East China University of Science & Technology, 130 Meilong Road, Shanghai 200237, China

Received 6 July 2005; revised 19 August 2005; accepted 20 August 2005

Available online 3 October 2005

Abstract—Molecular modeling and 3D-QSAR studies were performed on 31 indolomorphinan derivatives to evaluate their antagonistic behaviors on κ opioid receptor and provide information for further modification of this kind of compounds. Best predictions were obtained with CoMFA standard model ($q^2 = 0.693$, $N = 4$, $r^2 = 0.900$) and CoMSIA combined model ($q^2 = 0.617$, $N = 4$, $r^2 = 0.904$). Both models were further validated by an external test set of eight compounds with satisfactory predictions: $r^2 = 0.607$ for CoMFA and $r^2 = 0.701$ for CoMSIA. In addition, the 3D structure of human κ opioid receptor was constructed based on the crystal structure of bovine rhodopsin, and the CoMSIA contour plots were then mapped into the structural model of κ opioid receptor–GNTI complex to identify key residues, which might account for κ antagonist potency and selectivity. The roles of non-conserved Glu297 and conserved Lys227 of human κ opioid receptor were then discussed.

© 2005 Elsevier Ltd. All rights reserved.

1. Introduction

There are three well-adopted subtypes of opioid receptors: μ , κ , and δ .^{1,2} However, to date the precise role of κ opioid receptor has not been well established yet. It appears that κ opioid receptor exerts its physiological roles by participating in pain process and regulating immune systems^{3,4} where selective κ opioid antagonists could provide powerful tools to investigate detailed interactions between the receptor and ligand. Meanwhile, κ selective antagonists also showed some clinical potentials.^{5,6}

Nor-BNI (norbinaltorphimine, **1**) is the first highly selective κ opioid antagonist reported by Portoghese et al.,⁷ who believed that it was the second basic group that conferred κ potency and selectivity of the compound.⁸ The hypothesis was confirmed in their subsequent work⁹ by structure simplification of nor-BNI. The basic group was further identified interacting with Glu297 of κ opioid receptor by site-directed mutagenesis.¹⁰ Moreover, the attachment of a basic group to

the 5'-substitutes of naltrindole, a potent δ selective antagonist, led to the discovery of a more potent κ selective antagonist, 5'-guanidine naltrindole (GNTI, **2**).¹¹ There were also some other types of κ selective antagonists such as JDTC^{12,13} (**3**) and KAA-1(**4**)¹⁴ recently reported by Carroll and co-workers, which also owned a second basic group (Fig. 1).

In order to elucidate the mechanism of action of known kappa antagonists and design new kappa selective antagonists, molecular modeling and 3D-QSAR studies were conducted here. At first, 39 indolomorphinan derivatives, potent kappa selective antagonists by adding a basic or neutral group in the 5'-position of naltrindole, were collected from the literature. They were then divided into two groups: 31 compounds as training set and the other eight ones as test set. The training set was used to build 3D-QSAR models with CoMFA (comparative molecular field analysis) and CoMSIA (comparative molecular similarity indices analysis) methods, while the test set was used to validate the 3D-QSAR models further. Meanwhile, due to unavailability of experimental structure, the 3D structure of kappa opioid receptor was constructed based on the crystal structure of bovine rhodopsin. The interaction mode of GNTI with kappa receptor was hence obtained. Finally, the contour plots of CoMFA were mapped into the binding site of kappa receptor to identify key residues that might account for ligand binding and

Keywords: κ Opioid receptor; Indolomorphinan derivatives; 3D-QSAR; Molecular Modeling; CoMFA; CoMSIA.

*Corresponding authors. Tel.: +86 21 54237595; fax: +86 21 54237264 (Z.B.Q.); tel.: +86 21 54237419 (Y.T.); e-mail addresses: ytang234@yahoo.com.cn; zbqiu@shmu.edu.cn

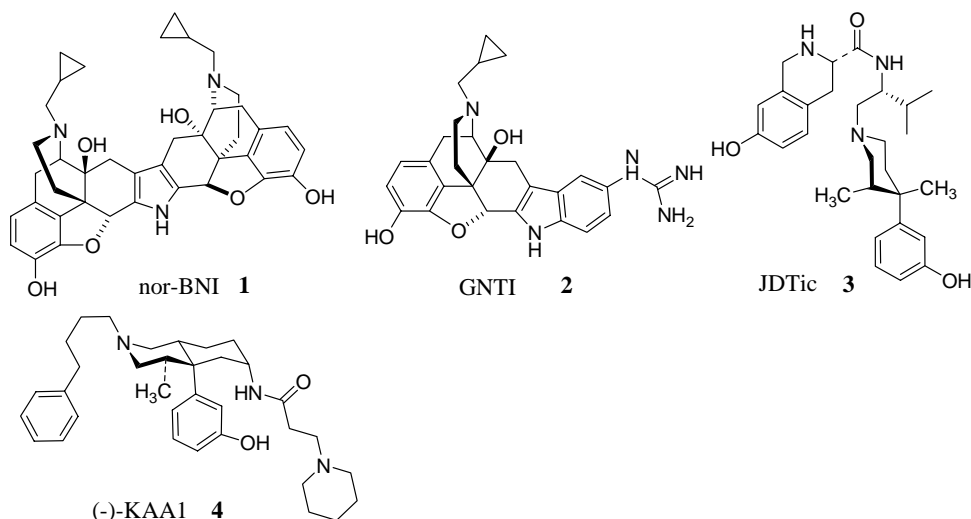


Figure 1. Some potent highly selective κ antagonists reported recently.

selectivity. The studies provided us helpful information on how to modify indolomorphinan derivatives.

2. Materials and methods

2.1. Data set

Thirty nine compounds were collected from several reports of the Lewis group^{15–18} (Table 1). Most of these compounds were indolomorphinan analogs of GNTI (2) and showed significant κ antagonistic potency, though they were also antagonists against μ and δ subtypes, too. All compounds were evaluated in competition binding assays with [³H] U69593 in cloned human κ opioid receptor transfected into Chinese hamster ovary (CHO) cells. Similar assays were also performed on GNTI by Jones and Portoghese.¹⁹ In this study, GNTI was only considered as a reference structure to eliminate evaluation errors between different groups. Eight compounds were randomly selected from the 39 molecules to make a test set for further model validation, and the rest of the 31 compounds served as the training set.

2.2. Molecular modeling and structural alignment

All calculations were carried out on a R14000 SGI Fuel workstation using molecular modeling software package SYBYL v6.9.²⁰ All compounds were constructed in SYBYL based on the crystal structure of nor-BNI²¹ since these compounds may similarly bind to κ opioid receptor. Considering the vital role of a basic group for κ selectivity and antagonistic potency, the basic groups of all compounds were fixed near the protonated nitrogen atom of nor-BNI supposing they shared similar binding models to κ opioid receptor. All compounds were protonated and assigned with Gasteiger–Hückel charges. For some more flexible compounds, systematic searches were performed with an interval of 10° on rotatory bonds to ensure their low energy conformations. Finally, they were minimized with Tripos force field.²²

The most crucial step in performing CoMFA and CoMSIA is to determine the bioactive conformations of the compounds so that all compounds could be aligned together. Though nor-BNI was not employed to establish 3D-QSAR models here, its structure was selected as the template for structural alignment from the alignment facility in SYBYL, due to its selective κ antagonistic potency and quite rigid structure. The final structural alignment is shown in Figure 2.

2.3. PLS analysis

As usual, PLS (partial least squares) method was used to establish and validate CoMFA and CoMSIA models here. The binding affinity K_i values were converted into pK_i values, to describe the biological activities. CoMFA was set at standard values, with a sp^3 carbon atom with one positive charge used to probe steric and electrostatic fields. The standard cutoff value was set to 30 kcal/mol. CoMSIA fields were set in their default opinions.

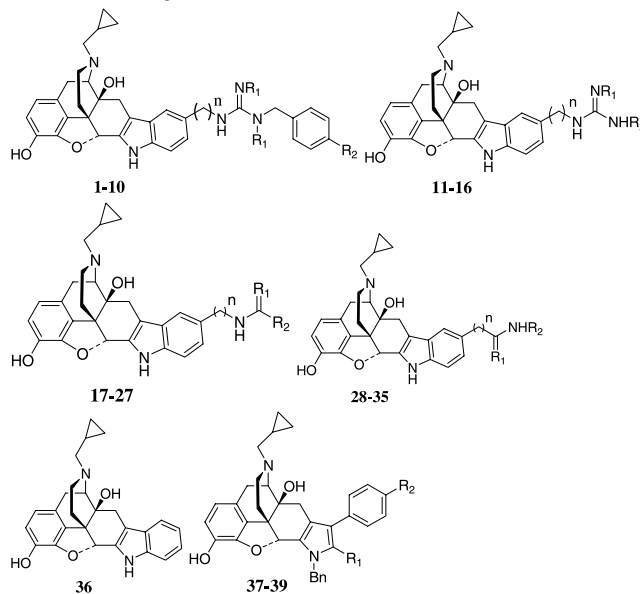
LOO (leave one out) cross-validation method was used to evaluate the initial models. The cross-validated coefficient q^2 was calculated using the following equation:

$$q^2 = 1.0 - \frac{\sum_{\gamma} (\gamma_{\text{pred}} - \gamma_{\text{actual}})^2}{\sum_{\gamma} (\gamma_{\text{actual}} - \gamma_{\text{mean}})^2}$$

where γ_{pred} , γ_{actual} , and γ_{mean} are predicted, actual, and mean values of the target property (pK_i), respectively, and $\text{PRESS} = \sum_{\gamma} (\gamma_{\text{pred}} - \gamma_{\text{actual}})^2$ is the sum of predictive sum of squares. The optimum number of components was then given, and CoMFA and CoMSIA models were hence derived corresponding to the optimum number. The parameters of confidence intervals were further estimated by bootstrap in 10 runs. The column filtering box was kept unchecked during all operations.

2.4. Validation of CoMFA and CoMSIA models

In addition to LOO method to validate the CoMFA and CoMSIA models, a test set made up of eight compounds

Table 1. Structures and binding affinities in the training set and test set

Compound	<i>n</i>	R ₁	R ₂	K _i (nM)
<i>Training set</i>				
1	2	H	H	1.42 ± 0.17
2	2	H	Cl	2.41 ± 0.22
3	2	H	NO ₂	2.14 ± 0.34
4	2	H	NH ₂	0.95 ± 0.04
5	0	H	H	0.86 ± 0.20
6	0	H	Cl	0.66 ± 0.05
8	0	H	NH ₂	0.63 ± 0.10
9	0	H	OH	3.26 ± 0.12
10	0	H	<i>m</i> -OH	2.74 ± 0.74
11	2	H	H	0.49 ± 0.00
13	0	<i>n</i> -Bu	<i>n</i> -Bu	6.96 ± 0.85
14	0	<i>n</i> -Pr	<i>n</i> -Pr	2.72 ± 0.39
15	0	<i>n</i> -Pr	CPM	2.38 ± 0.37
17	2	O	Et	1.57 ± 0.80
18	2	O	Pr	0.85 ± 0.40
19	2	O	Bu	0.68 ± 0.30
20	2	NH	Me	0.29 ± 0.10
22	2	NH	Pr	0.25 ± 0.10
23	2	NH	<i>n</i> -Bu	0.30 ± 0.20
24	2	NH	<i>i</i> -Bu	1.39 ± 0.14
26	2	O	NH- <i>n</i> -Bu	6.33 ± 0.40
27	2	O	NH- <i>n</i> -Hex	8.13 ± 2.67
29	1	NH	<i>n</i> -Pen	1.44 ± 0.04
30	1	NH	<i>n</i> -Hept	5.61 ± 0.37
31	0	O	<i>n</i> -Hept	21.89 ± 7.11
32	0	O	Bn	10.33 ± 0.66
34	0	O	(CH ₂) ₄ Ph	6.18 ± 0.47
35	0	O	<i>p</i> -MeO-Bn	2.11 ± 0.35
36				10.1 ± 0.65
38		CH ₃	H	183 ± 16
39		H	Pr	191 ± 3.9
<i>Test set</i>				
7	0	H	NO ₂	1.61 ± 0.45
12	2	<i>n</i> -Bu	<i>n</i> -Bu	4.80 ± 0.02
16	0	Bn	CPM	3.91 ± 0.60
21	2	NH	Et	0.28 ± 0.10
25	2	O	NH-Et	12.32 ± 1.29
28	1	NH	<i>n</i> -Pr	1.60 ± 0.28
33	0	O	(CH ₂) ₂ Ph	2.21 ± 0.35
37		H	H	120 ± 9.6

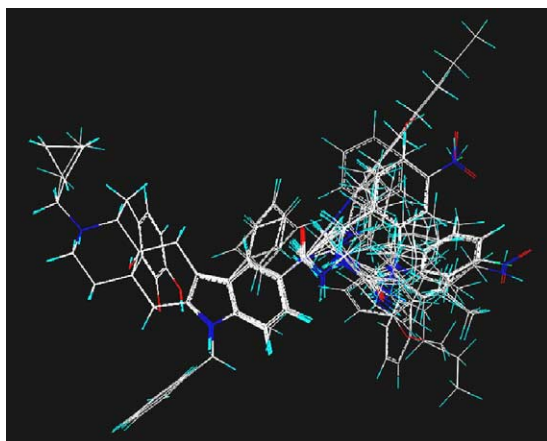


Figure 2. Superposition of 39 molecules including compounds in the training set and test set based on the template of nor-BNI, a potent and κ selective antagonist. (The structure of nor-BNI was removed for purposes of clarity.)

was used for model validation. Similar to cross-validated q^2 values of LOO method, the predictive performance of models on the test set was estimated by predictive r^2 values, which is expressed in the following equation:

$$\text{predictive } r^2 = \frac{\text{SSD} - \text{PRESS}}{\text{SSD}}$$

where SSD is the sum of squared deviation between the pK_i values of test set molecules and PRESS is the sum of squared deviations between the observed and the predicted pK_i values.

2.5. Homology modeling of kappa opioid receptor

The sequence of human kappa opioid receptor was retrieved from the SwissProt database (Accession No. P41145).²³ The sequences of bovine rhodopsin and human μ and δ opioid receptors were obtained from SwissProt, too, for sequence alignments (see Fig. 3). The crystal structure of bovine rhodopsin was retrieved from Protein Data Bank (PDB entry code 1F88),²⁴ which served as the template to generate the structural model of kappa opioid receptor. At first the 7 TM fragments were constructed by mutating the corresponding residue in the template into target residue in kappa receptor. Residue Ala106 was inserted into the target structure. The extracellular loop 2 (EL2), connecting TM4 and TM5, was built on the basis of EL2 of rhodopsin. The other extra- and intra-cellular loop regions were built with loop search function of SYBYL/Biopolymer module. The N- and C-terminal regions were extended from the transmembrane regions for 10 residues, not completely built. A disulfide bond was formed between the side chains of residues Cys131 and Cys210. After all done, adding all side chains and hydrogen atoms and loading Kollman All-Atom charges, the initial structure was energy minimized for 5000 steps with Kollman All-Atom force field.²⁵

The protonated GNTI was docked into the minimized structure of kappa receptor manually, by putting the protonated nitrogen toward the side chain of residue Asp138 and the guanidine group close to the side chain of Glu297. The whole complex structure was then min-

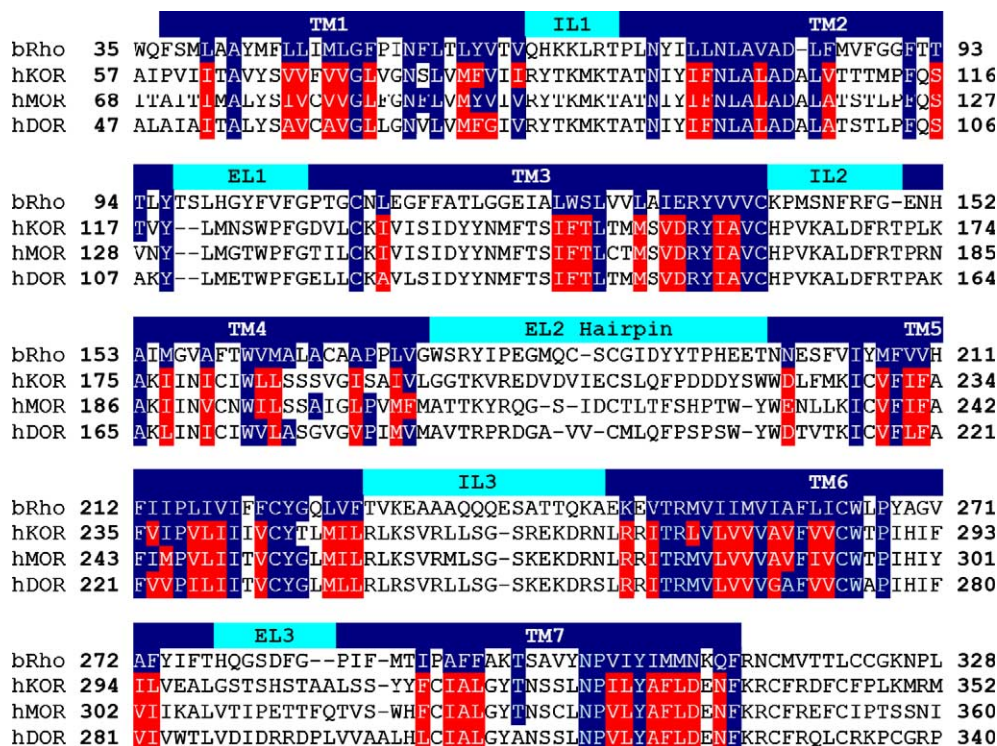


Figure 3. Sequence alignments of three subtypes of human opioid receptors with bovine rhodopsin (N- and C-terminals omitted). The transmembrane (TM) extracellular loop (EL), and intra-cellular loop (IL) regions were labeled correspondingly. In transmembrane regions, identical residues among them were highlighted in dark blue, while residues in opioid receptors analogous to those in rhodopsin were colored in red.

imized for 5000 steps again, with Tripos force field.²² The minimized GNTI–receptor complex structure was used for further analysis.

2.6. QSAR coefficient contour maps

CoMFA and CoMSIA results were visualized by 'stDev* Coeff' contours. The molecule-5 was visualized as the reference structure. Both CoMFA and CoMSIA plots were contoured by actual values. All the molecules used for QSAR analysis were aligned onto the GNTI structure in the GNTI–receptor complex, which led to the mapping of CoMSIA plots onto the bound receptor model. Key residues, which should account for κ selectivity and potency were hence recognized on the receptor model.

3. Results and discussion

3.1. Charge assignment of guanidine group

Charge assignment is crucial to a successful QSAR analysis, especially when molecules under investigation were positive charged or negative charged. In this study, many compounds contained a guanidine group with +1 charge, which was quite different from those mentioned in any other 3D-QSAR studies in the literature. Different from other groups like $-\text{NH}_3^+$, there are four central atoms, rather than one or two atoms, to share the one positive charge. How to correctly assign the one positive charge on each atom in guanidine group is quite challenging. Many methods led to different results, and different charge assignments led to different or even converse 3D-QSAR contours.

At first compounds with amino group in the study were set in their protonated type and fixed near the protonated nitrogen atom of nor-BNI. Various methods were used to calculate guanidine group charges such as Gasteiger,²⁶ Gasteiger–Hückel, Del Re,²⁷ MMFF94,^{28,29} Hückel,³⁰ and Pullman³¹ methods (Fig. 4). Based on different charge assignments on the guanidine group by various methods, the positive charges was focused on the central carbon atom, and the nearby three groups (each group composed of one nitrogen atom and two hydrogen atoms) showed a little negative charge to neutralize the highly positive

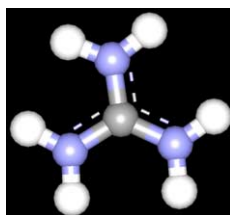
charged carbon atom in the center in MMFF94 and Del Re methods. Hückel calculation was questionable because of wrong nitrogen charge assignment. And one positive charge were distributed among three nearby groups with the central carbon little contribution to this charge in the Pullman method. However, Gasteiger–Hückel and Gasteiger calculations led to different results, in which the positive charge spread along the whole guanidine group. The carbon atom and three nearby groups made almost equal contributions to this one positive charge. Considering that the uniform charge distribution may be mostly preferable for guanidine group, Gasteiger–Hückel method was finally used in this study.

3.2. CoMFA and CoMSIA models and validation

The best predictions were obtained with CoMFA standard model ($q^2 = 0.693$, $N = 4$) and CoMSIA combined model with all descriptors ($q^2 = 0.617$, $N = 4$) (Table 2); their predictive performance on the test was $r^2 = 0.607$ by CoMFA and $r^2 = 0.701$ by CoMSIA, which indicated that the built 3D-QSAR models were reliable and able to predict binding affinities of new derivatives accurately. CoMSIA models with different field combinations were also evaluated by LOO and test set methodologies and these models also showed good predictive values (Table 2), which indicated that the CoMSIA models were less affected by fields employed. The conventional fit values on training set and prediction values on the test set made by the two models are shown in Table 3. The relationship curves between observed values versus conventional fit values (prediction values) on the training set (test set) are also displayed in Figure 5.

3.3. CoMFA and CoMSIA contours

CoMFA and CoMSIA contour plots showed that there was a large blue contour around the second basic group (Fig. 6a), which was in good agreement with previous reports^{8,10,11} and indicated that the positive-charged group in this region helped to increase binding affinity. However, a red contour was also observed in CoMSIA contour plots (Fig. 6b), which brought complexity to this region. A detailed analysis on electrostatic, steric, and hydrophobic (Fig. 6c) interactions of this kind of compounds is discussed below in combination with the κ opioid receptor model. Unlike other fields describing



	Gasteiger	Gasteiger–Hückel	Del-Re	MMFF94	Hückel	Pullman
C	+0.384	+0.286	+1.419	+1.200	-0.360	+0.059
H	+0.194	+0.261	+0.208	+0.450	0.000	+0.208
N	-0.183	-0.285	-0.555	-0.967	+0.453	-0.102

Figure 4. Different charge distributions of guanidine group calculated by multiple methods available in SYBYL. Carbon atoms were colored in gray, nitrogen atoms in blue, and hydrogen atoms in white.

Table 2. CoMFA and CoMSIA analysis on indolomorphinan κ antagonists

Model	q^2	N	r^2	SEE	F	SEEbs	q^2 bs	Pred. r^2
CoMFA(std)	0.693	4	0.900	0.238	58.245	0.188	0.924	0.607
CoMSIA(steric + electro)	0.738	6	0.923	0.217	47.651	0.150	0.964	0.579
CoMSIA(steric + electro + hydrophobic)	0.591	3	0.849	0.286	50.707	0.228	0.886	0.603
CoMSIA(steric + electro + hydrophobic + donor)	0.603	3	0.840	0.294	47.372	0.234	0.895	0.627
CoMSIA(steric + electro + hydrophobic + acceptor)	0.620	6	0.961	0.155	97.745	0.108	0.980	0.451
CoMSIA(all descriptors)	0.617	4	0.904	0.233	61.168	0.198	0.886	0.701

q^2 —leave one out (LOO) cross-validated correlation coefficient, N —optimum number of components, r^2 —noncross-validated correlation coefficient, SEE—standard error of estimate, F — F -test value, SEEbs—standard error of estimate by boot strapping analysis, q^2 bs—mean r^2 by boot strapping analysis (in 10 runs), Pred. r^2 —CoMFA (CoMSIA) predictive q^2 values on the test set.

Table 3. Actual versus conventional fit values (predicted values) activities of CoMFA (standard) and CoMSIA (all descriptors) models on the training set (test set)

Compound	Actual pK_i	CoMFA ^a		CoMSIA ^b	
		Conventional fit. ^c	Res ^d	Conventional fit ^c	Res ^d
<i>(a) Training set</i>					
Molecule-1	8.848	8.837	0.011	8.943	-0.095
Molecule-2	8.618	8.826	-0.208	8.889	-0.271
Molecule-3	8.670	8.828	-0.158	8.919	-0.249
Molecule-4	9.022	8.867	0.155	9.034	-0.012
Molecule-5	9.066	8.847	0.219	8.796	0.270
Molecule-6	9.181	8.967	0.214	8.802	0.379
Molecule-8	9.201	8.947	0.254	8.922	0.279
Molecule-9	8.487	8.880	-0.393	8.725	-0.238
Molecule-10	8.562	8.834	-0.272	8.673	-0.111
Molecule-11	9.310	9.315	-0.005	9.155	0.155
Molecule-13	8.157	8.157	0.000	8.421	-0.264
Molecule-14	8.565	8.446	0.119	8.481	0.084
Molecule-15	8.623	8.596	0.027	8.509	0.114
Molecule-17	8.804	9.084	-0.280	8.978	-0.174
Molecule-18	9.071	9.138	-0.067	9.042	0.029
Molecule-19	9.168	9.214	-0.046	9.108	0.059
Molecule-20	9.538	8.997	0.541	9.223	0.315
Molecule-22	9.602	9.266	0.336	9.391	0.211
Molecule-23	9.523	9.359	0.164	9.460	0.063
Molecule-24	8.857	9.156	-0.299	9.331	-0.474
Molecule-26	8.199	8.221	-0.022	8.175	0.024
Molecule-27	8.090	8.031	0.059	7.962	0.128
Molecule-29	8.842	8.645	0.197	8.709	0.133
Molecule-30	8.251	8.558	-0.307	8.671	-0.420
Molecule-31	7.660	7.722	-0.062	7.759	-0.099
Molecule-32	7.986	8.401	-0.415	8.172	-0.186
Molecule-34	8.209	8.218	-0.009	8.081	0.128
Molecule-35	8.676	8.501	0.175	8.384	0.292
Molecule-36	7.996	8.100	-0.104	8.135	-0.139
Molecule-38	6.738	6.635	0.103	6.715	0.022
Molecule-39	6.719	6.642	0.077	6.670	0.049
<i>(b) Test set</i>					
Compound	Actual pK_i	CoMFA ^a		CoMSIA ^b	
		Predicted pK_i ^c	Res ^d	Predicted pK_i ^c	Res ^d
Molecule-7	8.793	8.943	-0.150	8.547	0.246
Molecule-12	8.319	8.659	-0.340	8.677	-0.358
Molecule-16	8.408	8.806	-0.398	8.549	-0.142
Molecule-21	9.553	9.180	0.373	9.335	0.218
Molecule-25	7.909	8.671	-0.761	8.415	-0.505
Molecule-28	8.796	8.537	0.259	8.675	0.121
Molecule-33	8.656	7.977	0.679	7.832	0.824
Molecule-37	6.921	6.630	0.291	6.743	0.178

^a CoMFA standard model.

^b CoMSIA model combined with all descriptors.

^c Conventional fitted value.

^d Difference between actual and fitted (predicted) pK_i values.

^e Predicted pK_i value.

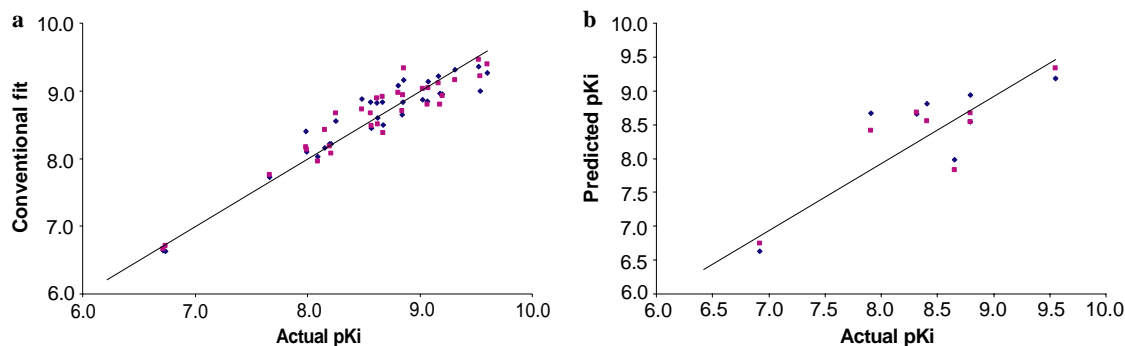


Figure 5. Plot of observed pK_i versus conventional fit predictions (predicted activities) of training set (a) and test set (b). Blue rhombs show conventional fit (predictions) of CoMFA standard model and pink triangles show those of CoMSIA (all descriptors) model.

compound binding requirements, H-bond fields describe properties located on the receptor. In H-bond donor field contours, areas colored in cyan where H-bond acceptors on the receptor are predicted to favor binding and areas colored in purple where H-bond acceptors on the receptor are predicted to reduce binding. For acceptor field contours, it shows regions where H-bond donors on the receptor are predicted to enhance (magenta) and reduce (red) binding capacity. H-bond donor/acceptor contour maps (Fig. 6d and e) suggested that there should be one H-acceptor and one H-donor favored for binding in the receptor.

3.4. Homology modeling of kappa opioid receptor and GNTI-receptor complex

Currently there is only one crystal structure, that is, bovine rhodopsin, belonging to the superfamily of G-protein coupled receptors (GPCR). Because the seven transmembrane regions are highly conserved among the whole family, the structure of bovine rhodopsin has been hence widely used as a template to model 3D structures of any other GPCR (for a recent review, please see Ref. 32). Excellent results, such as successful virtual screening, have already been obtained based on rhodopsin-derived structural models.^{33,34} Kappa opioid receptor belongs to the superfamily of GPCR, therefore, it is reasonable to construct its structural model based on the unique crystal structure of bovine rhodopsin.

Because of the long sequence and importance of the extracellular loop 2, it is difficult to model a reliable structure by the loop search method. There was only one residue number difference between the two sequences, hence, the EL2 of rhodopsin was used as a template to model the EL2 region of the receptor.

The binding site of GNTI was determined according to experimental evidence, such as site-directed mutagenesis results. Because the supposed binding pocket of the receptor was not enough to accommodate GNTI, the ligand was docked into the binding pocket of the model manually, and some side chains of residues around GNTI were adjusted to release more space for the ligand. After energy minimization, the ligand-receptor complex was formed. Binding residues including Asp138, Glu297, and Tyr312, which formed key interac-

tions with GNTI, were consistent with experimental evidence. In addition to the interactions reported in the literature,¹¹ two novel hydrogen bonds were identified in our model. The oxygen bridge between C4 and C5 in GNTI structure formed a hydrogen bond with Tyr139. Another hydrogen bond was observed between the guanidine with Tyr312. Therefore, the GNTI-receptor complex structure was a reasonable model to map CoMSIA contours and identify the binding features of indolomorphinan derivatives.

3.5. Mapping CoMSIA contours in the GNTI-receptor complex model

Based on the above 3D-QSAR models, the CoMSIA contours were further mapped into a κ opioid receptor model (Fig. 7a), the blue mesh (Fig. 7b) generated by CoMSIA, meant positive charge would be favorable for binding affinity, was exactly located around negative-charged residue Glu297, which indicated the importance of residue Glu297 in antagonist binding and was consistent with experimental evidence. The corresponding residue of Glu297 in κ subtype was Trp284 in δ and Lys305 in μ subtypes, respectively, quite different among them. Therefore, Glu297 would not only contribute to the binding affinity, but also to the selectivity. Besides, this blue region extended to Tyr312, indicating that residue Tyr312 might get involved in antagonist binding, too. However, when this residue was replaced by alanine,³⁵ the binding affinities of GNTI and nor-BNI to κ opioid receptor increased slightly, so it is hard to address the role of Tyr312 upon antagonist binding exactly here.

Meanwhile, the red meshes, meant negative charge favorable to binding affinity, were observed to match the positive-charged residue Lys227 (Fig. 7b), which suggested Lys227 plays a role in antagonist binding. This result was further confirmed by H-bond acceptor contours (Fig. 6e) where one H-bond donor favored for binding may exist in this area of the receptor. Obviously, this H-bond donor refers to the residue Lys227. Nevertheless, this residue is highly conserved among all the three opioid receptors, and the assumption that all naltrexone derived compounds bind to opioid receptors in similar modes was widely accepted.³⁵ Compounds interacting with this residue may also increase

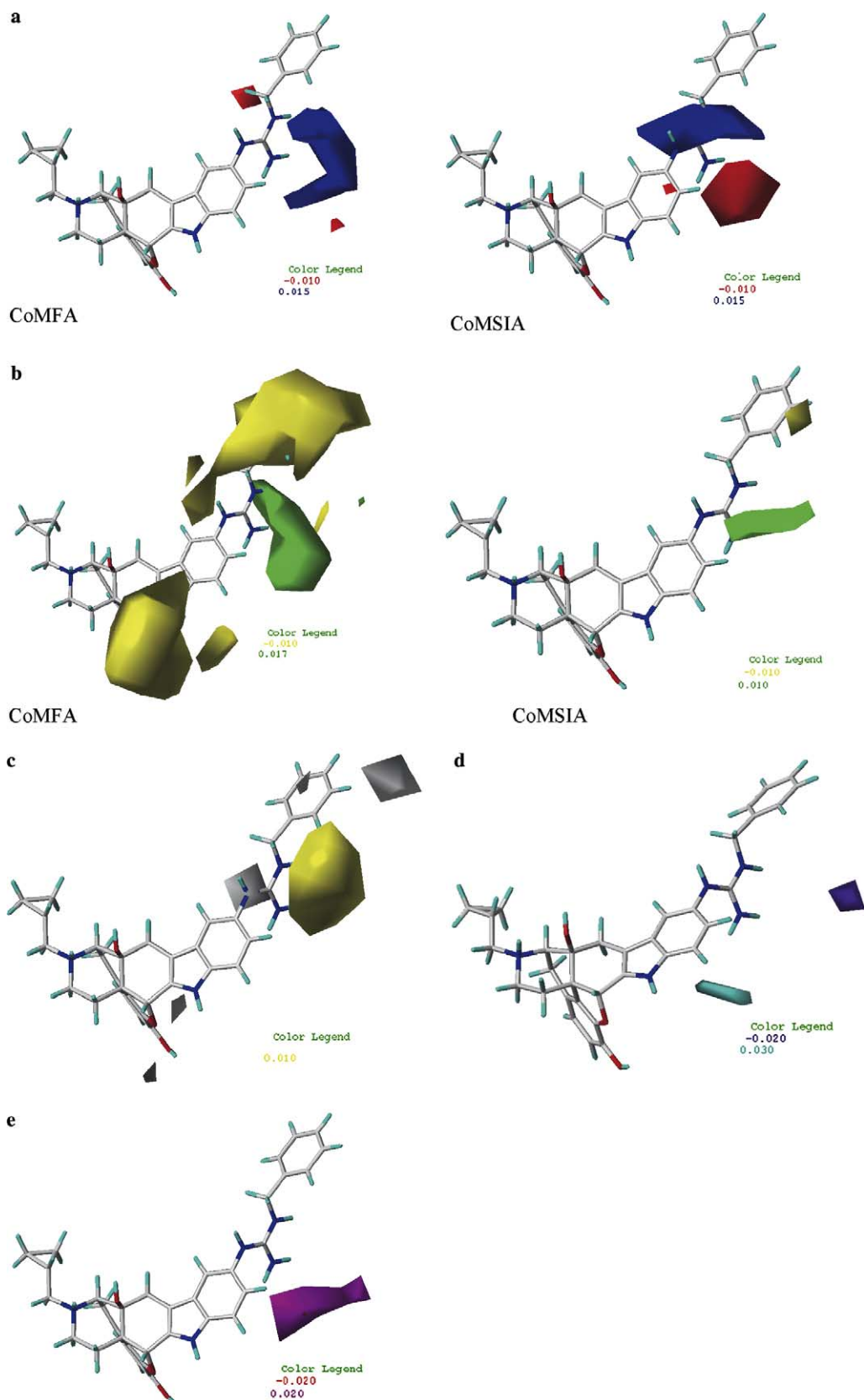


Figure 6. CoMFA (standard model) and CoMSIA (all descriptors model) $\text{stdev}^* \text{coeff}$ Contour plots: (a) red contours predict negative charge enhance affinity, whereas blue contours predict positive charge enhance affinity; (b) green contours predict bulky group enhance affinity, whereas yellow contours predict less bulky group is favored for affinity; (c) yellow contours predict hydrophobes enhance affinity, whereas white contours predict hydrophilic group enhance affinity; (d) cyan contours predict H-bond acceptors on the receptor enhance binding, whereas purple contours reduce binding; (e) magenta contours predict H-bond donors on the receptor enhance binding, whereas red contours reduce binding.

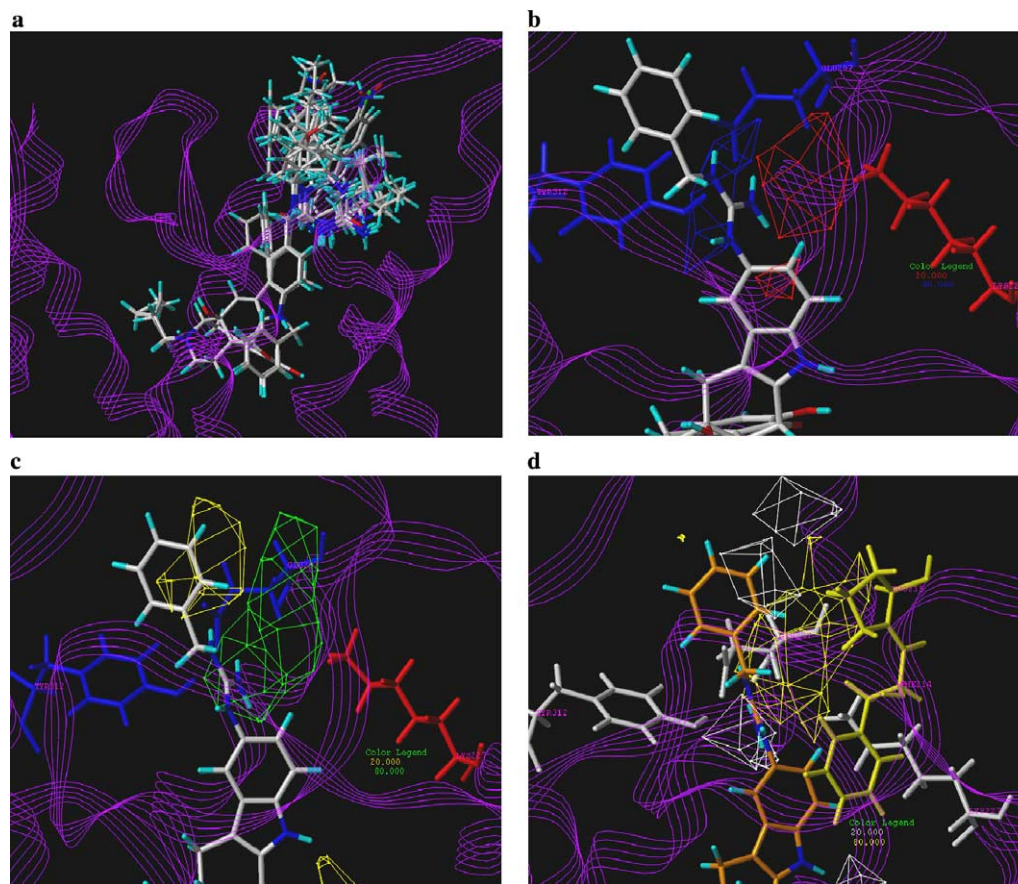


Figure 7. (a) Structural aligned compounds were mapped to the modeled κ opioid receptor–GNTI complex; (b) electrostatic contours: red mesh predict negative charge enhance affinity, whereas blue mesh predict positive charge enhance affinity; (c) steric contours: green mesh predict bulk favored for binding affinity, whereas yellow mesh predict bulky group reduce binding; (d) hydrophobic contours: yellow mesh predict hydrophobic group enhance binding, whereas white mesh predict hydrophilic group enhance binding. (Nearby hydrophobic residues are colored in yellow and polar residues in white.)

their binding affinity to other two opioid receptors. Hence, it is reasonable to suppose that residue Lys227 mainly contributes to the binding affinity but has nothing to do with the selectivity.

Some compounds (compounds **17–19**) containing only neutral amide groups rather than basic groups also showed considerable κ binding affinity and antagonist potency. They displayed their antagonist potency in [^{35}S]GTP γ S assays by compound **17** ($K_e = 0.48$ nM), compound **18** ($K_e = 0.35$ nM), and compound **19** ($K_e = 0.46$ nM), respectively (nor-BNI $K_e = 0.04$ nM as control).¹⁵ However, these compounds showed almost no selectivity between κ and δ , especially in antagonist potency assays *in vitro*. Therefore, it was obvious that a basic group interacting with Glu297 was essential to the selectivity of κ antagonist, and once again residue Lys227 had nothing to do with the selectivity. In addition, Black¹⁵ proposed that the highly electronegative oxygen atom in amide group may interact with Lys214 in δ receptor (identical to Lys227 in κ receptor) by H-bond and thus increase their binding affinity to δ receptor, which was also in good agreement with our results.

In steric contour meshes (Fig. 7c), green ones, indicating that more bulky would be favorable for binding affinity,

extended along binding gorge. It was worthy to note that one yellow area, being less bulky for binding affinity, occupied near Glu297 and Tyr312. Just as Metzger et al.³⁵ explained in mutation studies on κ opioid receptor, the replacement of the bulky Tyr312 with less bulky alanine may actually facilitate binding.

We also mapped hydrophobic contours (Fig. 7d) into the κ receptor. Polar residues around regions were colored in white and hydrophobic residues in yellow. Several hydrophilic areas were proposed where Tyr312, Glu297, and space along the gorge tunnel were present. Furthermore, Phe214 and Pro215 of second extracellular loop (EL-2) may also account for hydrophobic interactions with antagonists in the κ opioid receptor.

Combining all the above mapping information, it was believed that, when modifying the 5'-position of naltrindole, a less bulky but hydrophilic group, better a small basic group toward Glu297 and Tyr312 would increase the binding affinity and κ selectivity; on the other side, a big and hydrophobic fragment with partial negative charge would form hydrophobic interactions with residues Phe214 and Pro215 and hydrogen-bonding interaction with Lys227.

4. Conclusion

3D-QSAR models of indolomorphinan derivatives were obtained by CoMFA and CoMSIA methods. Both of them showed good predictive capabilities for antagonist binding upon κ opioid receptors. Based on the results, CoMSIA contours were further mapped into the κ opioid receptor–GNTI complex model and several key residues were identified. The results demonstrated that a second basic group was essential to κ selectivity and residue Glu297 was crucial for κ antagonist potency and selectivity, whereas residue Lys227 of κ opioid receptor was identified to contribute to antagonist's binding affinity rather than selectivity due to its conservation among all three opioid receptors. At last a suggestion on how to modify the structure of indolomorphinan was given.

References and notes

- Gilbert, P. E.; Martin, W. R. *J. Pharmacol. Exp. Ther.* **1976**, *198*, 66.
- Martin, W. R.; Eades, C. G.; Thompson, J. A.; Huppler, R. E.; Gilbert, P. E. *J. Pharmacol. Exp. Ther.* **1976**, *197*, 517.
- Ackley, M. A.; Hurley, R. W.; Virnich, D. E.; Hammond, D. L. *Pain* **2001**, *91*, 377.
- Fields, H. *Nat. Rev. Neurosci.* **2004**, *5*, 565.
- Vink, R.; Portoghese, P. S.; Faden, A. I. *Am. J. Physiol.* **1991**, *261*, R1527.
- Mague, S. D.; Pliakas, A. M.; Todtenkopf, M. S.; Tomasiewicz, H. C.; Zhang, Y.; Stevens, W. C., Jr.; Jones, R. M.; Portoghese, P. S.; Carlezon, W. A., Jr. *J. Pharmacol. Exp. Ther.* **2003**, *305*, 323.
- Portoghese, P. S.; Lipkowski, A. W.; Takemori, A. E. *Life Sci.* **1987**, *40*, 1287.
- Portoghese, P. S.; Nagase, H.; Takemori, A. E. *J. Med. Chem.* **1988**, *31*, 1344.
- Lin, C. E.; Takemori, A. E.; Portoghese, P. S. *J. Med. Chem.* **1993**, *36*, 2412.
- Larson, D. L.; Jones, R. M.; Hjorth, S. A.; Schwartz, T. W.; Portoghese, P. S. *J. Med. Chem.* **2000**, *43*, 1573.
- Stevens, W. C., Jr.; Jones, R. M.; Subramanian, G.; Metzger, T. G.; Ferguson, D. M.; Portoghese, P. S. *J. Med. Chem.* **2000**, *43*, 2759.
- Thomas, J. B.; Atkinson, R. N.; Vinson, N. A.; Catanzaro, J. L.; Perretta, C. L.; Fix, S. E.; Mascarella, S. W.; Rothman, R. B.; Xu, H.; Dersch, C. M.; Cantrell, B. E.; Zimmerman, D. M.; Carroll, F. I. *J. Med. Chem.* **2003**, *46*, 3127.
- Carroll, I.; Thomas, J. B.; Dykstra, L. A.; Granger, A. L.; Allen, R. M.; Howard, J. L.; Pollard, G. T.; Aceto, M. D.; Harris, L. S. *Eur. J. Pharmacol.* **2004**, *501*, 111.
- Thomas, J. B.; Atkinson, R. N.; Namdev, N.; Rothman, R. B.; Gigstad, K. M.; Fix, S. E.; Mascarella, S. W.; Burgess, J. P.; Vinson, N. A.; Xu, H.; Dersch, C. M.; Cantrell, B. E.; Zimmerman, D. M.; Carroll, F. I. *J. Med. Chem.* **2002**, *45*, 3524.
- Black, S. L.; Jales, A. R.; Brandt, W.; Lewis, J. W.; Husbands, S. M. *J. Med. Chem.* **2003**, *46*, 314.
- Black, S. L.; Chauvignac, C.; Grundt, P.; Miller, C. N.; Wood, S.; Traynor, J. R.; Lewis, J. W.; Husbands, S. M. *J. Med. Chem.* **2003**, *46*, 5505.
- Srivastava, S. K.; Husbands, S. M.; Aceto, M. D.; Miller, C. N.; Traynor, J. R.; Lewis, J. W. *J. Med. Chem.* **2002**, *45*, 537.
- Grundt, P.; Martinez-Bermejo, F.; Lewis, J. W.; Husbands, S. M. *J. Med. Chem.* **2003**, *46*, 3174.
- Jones, R. M.; Portoghese, P. S. *Eur. J. Pharmacol.* **2000**, *396*, 49.
- SYBYL: Tripos Inc, 6.9 ed., 1699 Hanley Road, St. Louis, MO 63144.
- The crystal structure of nor-BNI was obtained from <http://www.opioid.umn.edu>.
- Clark, M.; Cramer, R. D. I.; van Opdenbosch, N. *J. Comput. Chem.* **1989**, *10*, 982.
- Bairoch, A.; Apweiler, R. *Nucleic Acids Res.* **2000**, *28*, 45.
- Palczewski, K.; Kumasaka, T.; Hori, T.; Behnke, C. A.; Motoshima, H.; Fox, B. A.; Le Trong, I.; Teller, D. C.; Okada, T.; Stenkamp, R. E.; Yamamoto, M.; Miyano, M. *Science* **2000**, *289*, 739.
- Hall, D.; Pavitt, N. *J. Comput. Chem.* **1984**, *5*, 441.
- Gasteiger, J.; Marsili, M. *Tetrahedron* **1980**, *36*, 3219.
- Del Re, G. *J. Chem. Soc.* **1958**, 4031.
- Halgren, T. A. *J. Comput. Chem.* **1996**, *17*, 490.
- Halgren, T. A. *J. Comput. Chem.* **1996**, *17*, 553.
- Purcel, W.; Singer, J. *J. Chem. Eng. Data* **1967**, *12*, 235.
- Berthod, H.; Pullman, A. *J. Chem. Phys.* **1965**, *62*, 942.
- Stenkamp, R. E.; Teller, D. C.; Palczewski, K. *Arch. Pharm. Chem. Life Sci.* **2005**, *338*, 209.
- Evers, A.; Klebe, G. *Angew. Chem., Int. Ed.* **2004**, *43*, 248.
- Evers, E.; Klabunde, T. *J. Med. Chem.* **2005**, *48*, 1088.
- Metzger, T. G.; Paterlini, M. G.; Ferguson, D. M.; Portoghese, P. S. *J. Med. Chem.* **2001**, *44*, 857.